Fluorographane : a promising material for bipolar doping of MoS_2

Fluorographane: a promising material for bipolar doping of MoS_2 †

Deniz Çakır,*[a] and Francois M. Peeters[a]

Received Xth January 2015, Accepted Xth XXXXXXXXX 20XX
First published on the web Xth XXXXXXXXXX 200X
DOI: 10.1039/b000000x

Using first principles calculations we investigate the structural and electronic properties of interfaces between fluorographane and MoS_2. Unsymmetrical functionalization of graphene with H and F results in an intrinsic dipole moment perpendicular to the plane of the buckled graphene skeleton. Depending on the orientation of this dipole moment, the electronic properties of a physically absorbed MoS_2 monolayer can be switched from *n*- to *p*-type or vice versa. We show that one can realize vanishing *n*-type/*p*-type Schottky barrier heights when contacting MoS_2 to fluorographane. By applying a perpendicular electric field, the size of the Schottky barrier and the degree of doping can be tuned. Our calculations indicate that a fluorographane monolayer is a promising candidate for bipolar doping of MoS_2, which is vital in the design of novel technological applications based on two-dimensional materials.

1 Introduction

Transition metal dichalcogenides (TMDCs) are a large family of layered materials with diverse electronic, thermal, magnetic and mechanical properties [1–11]. TMDCs are expected to be used in various technological applications including catalysis [8], energy storage [12], sensing [9], and electronic devices such as field-effect transistors (FETs) [13–16] and logic circuits [4,9]. The performance of the TMDC based device applications is strongly influenced by the interfaces between TMDCs and metal electrodes. Thus, a detailed knowledge of the electronic properties of the interface between TMDCs and metal electrodes is essential in order to implement TMDCs in efficient device applications. The interface between a two-dimensional (2D) material and a metal electrode plays a key role in the performance of a device constructed from low-dimensional materials because the injection, collection, concentration, and mobility of the charge carriers are mainly determined by the interfaces [17–24].

Previous experimental works and theoretical calculations have suggested that the metal-TMDC interface suffers from the presence of a Schottky barrier that results in a higher contact resistance which obstructs the carrier injection across the interface [17]. Such Schottky barriers have been considered to originate from the pinning of the Fermi level close to the conduction band of TMDCs. The origin of the Fermi level pinning has been attributed to the modification of the metal work function by the formation of an interface dipole due to the charge redistribution and the formation of gap states. In the case of MoS_2, the latter are mainly of Mo *d*-orbitals character [25]. Different scenarios have been proposed to eliminate the Fermi level pinning at the interface. A remedy to mitigate the Fermi level pinning has been proposed in Refs. 26 and 27. They suggested the insertion of a thin oxide layer that acts as a tunnel barrier between the metal electrode and TMDCs, thereby lowering the Schottky barrier height at the metal-TMDCs interface. Alternatively, Cakir *et al.* proposed to use self-assembled monolayers (SAMs) instead of oxides in order to control the Schottky barrier height and the energy level alignment (i.e., position of the metal Fermi level relative to either valence or conduction band edge of the TMDC) at the interface [28]. Depending on the type of SAMs, it is also possible to dope TMDCs either *n*-type or *p*-type.

Another difficulty with TMDC/metal interfaces is to achieve a *p*-type contact. For instance, while MoS_2 is a promising model system for applications in optoelectronic devices and FETs, its practical use has been restricted to *n*-type transistors [13,29]. Even if high work function metals are used, MoS_2/metal interfaces mostly show a *n*-type Schottky contact. Such behavior hampers the use of TMDCs in logic circuits since it is necessary to fabricate both *n*- and *p*-type FETs. Interfacing TMDCs with other 2D materials could result in *p*-type doping of TMDCs. Similarly, to realize a vanishing Schottky barrier height at the interface one can insert another 2D material between the metal electrode and TMDC [30,31]. Musso *et al.* demonstrated that a single layer of graphene-oxide forms a *p*-type contact with MoS_2 and the size of the Schottky barrier at the interface can be tuned by changing the concentration of oxygen [32]. Moreover, interfacing MoS_2 with graphene-oxide instead of traditional metals weakens the Fermi level pinning at the graphene-oxide/MoS_2 interface. Due to the lack of dangling bonds, individual 2D materials preserve their physical and chemical properties in

[a] *Department of Physics, University of Antwerp, Groenenborgerlaan 171, 2610 Antwerpen, Belgium; E-mail: dcakir79@gmail.com; E-mail:francois.peeters@uantwerpen.be*

heterostructures.

In order to control or modify the physical and chemical properties of graphene[33–35], doping with foreign atoms appears as a promising approach. So far, synthesis of hydrogenated graphene, fluorographene, and chlorographene have been achieved. Theoretical calculations have suggested that interesting theoretical materials can be obtained via functionalization of graphene[36]. Among them, fluorographane is obtained by adsorption of H and F atoms on opposite sides of graphene[37–40]. Recently, the piezoelectric potential of fluorographane has been shown using first principles calculations[41,42].

In this study, we found that contacting MoS_2 to a fluorographane monolayer is a promising strategy for the design of interfaces with zero Schottky barrier height. In addition, bipolar doping of MoS_2 is achievable depending on which side fluorographane is interfaced with the MoS_2 monolayer. We also show that the Schottky barrier height and hence the degree of *n*- or *p*-type doping of MoS_2 can be tuned by using an out of plane electric field.

2 Computational Methodology

First principles calculations based on density functional theory are carried out by using the Vienna ab initio simulation package (VASP)[43,44] code using the GGA-PBE[45] functional to treat the electronic exchange correlation interaction. The projected augmented-wave (PAW) method is used to describe the electron and ion interaction. Plane waves up to a kinetic energy cutoff of 400 eV are included in the calculations. For the structure optimizations, the Brillouin zone is sampled by a Γ centered 2×2×1 *k*-point mesh within the Monkhorst-Pack scheme[46]. To get accurate band structures, each high symmetry direction in the Brillouin zone is sampled by using 12 *k* points. We assume convergence when the difference of the total energies between two consecutive ionic steps is less than 10^{-5} eV and the maximum force allowed on each atom is 0.01 eV/Å. A vacuum region of at least 20 Å along the *z*-direction is used to separate the periodic images in order to avoid spurious interactions. To prevent interaction between the dipoles of repeated slabs, we include a dipole correction in the calculations. To obtain the electrostatic potential, and hence the potential drop at the interface, we calculate the plane averaged potential along the surface normal by using the following expression,

$$\overline{V}(z) = \frac{1}{A}\int\int_{cell} V(x,y,z)dxdy, \quad (1)$$

where A is the area of the surface unit cell. Since the semi-local functionals such as GGA fail to describe weakly interacting systems, we also take into account the van der Waals (vdW) interaction within the Grimme approach to provide a better description of the interfaces between the weakly interacting structures[47]. All the pair interactions up to a radius of 25 Å are included in the calculations.

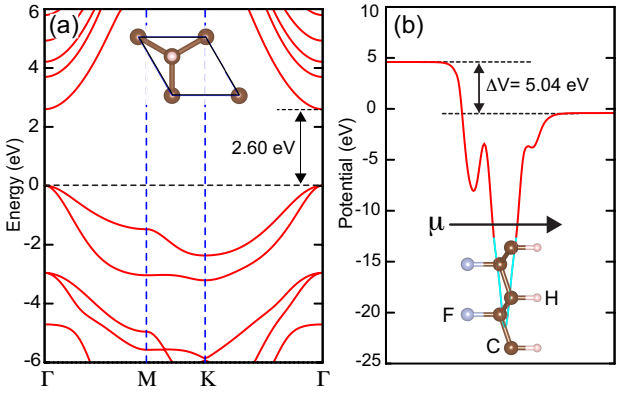

Fig. 1 (a) Calculated band structure of bare fluorographane and (b) plane averaged electrostatic potential energy across bare fluorographane. Black arrow shows the direction of the dipole moment.

3 Pristine fluorographane

We first investigate the structural and electronic properties of bare fluorographane. Our GGA-PBE calculations predict that fluorographane is a direct band gap semiconductor at the Γ-point with a band gap of 2.6 eV, see Fig. 1(a). Absorption of H and F atoms on graphene results in a buckled structure (with a buckling distance of 0.48 Å) and enlarges the lattice parameter of graphene from 2.54 to 2.57 Å, (see inset of Fig. 1(b)). The C-C, C-H and C-F bond lengths are 1.56, 1.11 and 1.38 Å, respectively. Alternating decoration of pristine graphene with H and F atoms on alternating sides of graphene (see inset of Fig. 1(a)) converts the sp^2 hybridization to sp^3. Because the H and F atoms are located on opposite sites of the buckled graphene plane, we observe a very large potential step of 5.04 eV along the direction perpendicular to fluorographane, see Fig. 1(b) for the plane averaged electrostatic potential energy across pristine fluorographane. Such a potential drop develops a dipole moment, pointing from the F-side to the H-side.

4 Fluorographane-MoS_2 bilayer heterostructure

Next, we study the structural and electronic properties of the heterostructure made of fluorographane and a monolayer of MoS_2. In order to construct an appropriate supercell with a minimal lattice mismatch, we consider an interface between a 5×5 fluorographane and a 4×4 layer of MoS_2. In this particular geometry, the calculated lattice mismatch between flu-

orographane and MoS_2 is about 2 %. The lattice parameter of fluorographane is forced to be commensurable to the lattice of MoS_2. In the construction of the heterostructure between fluorographane and MoS_2, we consider the electronegativity of the atoms. Since the F and S atoms carry a negative net charge, they avoid each other. In order to get a realistic stacking, we minimize the direct F-S interactions at the interface. In other words, we maximize the interatomic distances between the F and S atoms. In contrast, H carries a positive net charge such that it prefers to stay close to the S atoms. It is possible that the interface structure between fluorographane and MoS_2 is not the lowest energy structure due to the existence of a large number of possible stacking configurations. For this purpose, we performed calculations for very different stacking configurations and found that there is no significant change in the calculated electronic properties. In addition, in a recent work, an ultra smooth potential energy surface was predicted at the fluorographene-MoS_2 interface in the context of a study on friction, meaning that different stacking structures result in similar energetic.[48]

Since fluorographane has two different terminations, two different kinds of heterostructures are possible. In the first (second) heterostructure, MoS_2 is placed on the hydrogen (fluorine) terminated side of fluorographane, as depicted in Fig. 2(a) and Fig. 2(b). In the GGA + vdW optimized structures, the distance between the two planes formed by Mo atoms of the MoS_2 and the midway of buckled C layers is around 6 Å. Apart from structural differences between the two heterostructures, the orientation of the intrinsic dipole moments is opposite with respect to MoS_2, which is expected to result in different electronic properties. For both types of heterostructures, we compute the band structure and obtain the *n*- and *p*-type Schottky barrier heights for MoS_2, see Fig. 2(c) and Fig. 2(d). The *n*-type Schottky barrier height (Φ_n) is defined as the energy difference between the Fermi level and the minimum of the conduction band of MoS_2 contacted to the hydrogenated side of fluorographane. For the system in which MoS_2 is contacted to the fluorinated side of fluorographane, the Fermi level of the combined system appears between the valence band of MoS_2 and the conduction band of fluorographane. For such a system, we define the *p*-type Schottky barrier height (Φ_p) as the energy difference between the minimum of the conduction band of fluorographane and the valence band of MoS_2. The first clear observation is that the position of the Fermi level with respect to the band edges of MoS_2 is totally different. Since MoS_2 is physisorbed on fluorographane, the band structure of MoS_2 is nearly unperturbed. Placing MoS_2 on the hydrogen terminated side of fluorographane yields a *n*-type zero Schottky barrier height. However, as one rotates the dipole of fluorographane by 180° (i.e., putting MoS_2 on the fluorine terminated side) the Fermi level appears very close to the top of the valence band, indicating a very strong *p*-type doping of the MoS_2 monolayer. The *p*-type Schottky barrier height is found to be 0.16 eV. This means that thermionic emission may obscure such a small Schottky barrier height at finite temperatures[49]. As is clear that by changing the orientation of the intrinsic dipole moment of fluorographane with respect to MoS_2, the type of doping of MoS_2 can be switched from *n*- to *p*-type or vice versa. Without needing an external electric field, we can achieve zero or small Schottky barriers at the interfaces. This controllable doping of MoS_2 allows for the fabrication of MoS_2 based *p-n* junctions and transistors.

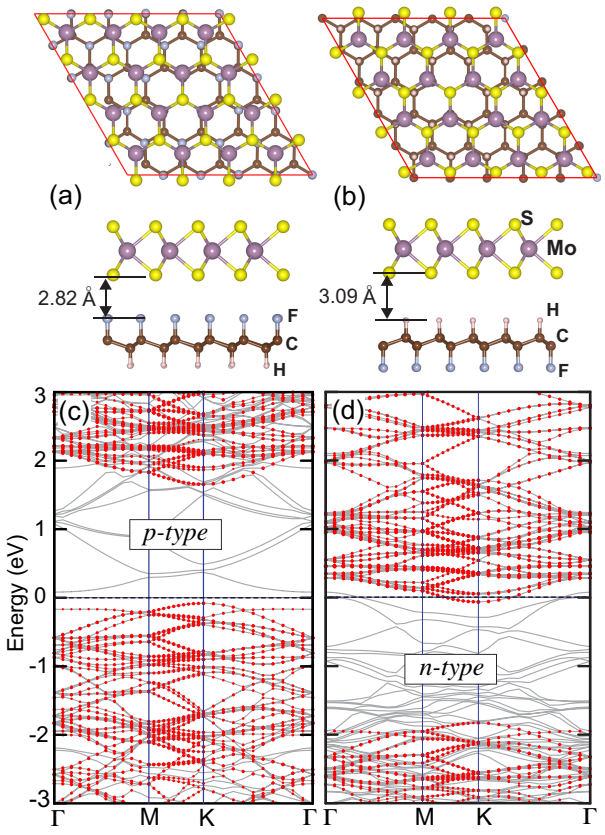

Fig. 2 Top and side views of the fluorographane-MoS_2 herestructures for F-side (a) and H-side (b) towards MoS_2 and their corresponding band structures in (c) and (d). Red filled circles are used to show the band structure of MoS_2. Fermi level is at 0 eV.

To explain Fermi level pinning, different mechanisms have been proposed. Among them, the role of surface states in the pinning of the Fermi level in the band gap of semiconductors was emphasized by Bardeen. The metal-induced gap states mechanism[50] can be directly correlated to the interfacial gap states that are basically metallic wave functions decaying into the semiconductor[51]. In addition, the presence of defect/disorder may result in a high density of interface states at the metal-semiconductor interfaces[52]. In contrast to the

standard metal-TMDC interfaces (for instance Sc-TMDC[24]), due to the presence of the weak van der Waals interaction, the fluorographane-MoS_2 interface is free of interface states within the band gap of MoS_2, which are considered as one of the main origins of Fermi level pining. Consequently, the fluorographane-MoS_2 interface does not suffer from Fermi level pinning. It is evident that exfoliated or chemically growth MoS_2 is not absolutely free of defects that may result in Fermi level pinning at the fluorographane-MoS_2 interface. The presence of defects (for instance S vacancy on MoS_2) may lead to localized states within the band gap of MoS_2, at which the Fermi level may be pinned[53–56]. Thus, the success of proposed fluorographane-MoS_2 heterostructures is largely dependent on the quality of the MoS_2 and fluorographane monolayers.

It is worth mentioning that the band gap of fluorographane is quite sensitive to the type of stacking. In a previous study, it was shown that while the monolayer of fluorographane is a semiconductor with a band gap of 2.83 eV, bilayer fluorographane exhibits metallic behavior[57]. This is because the uncompensated depolarization field, originating from the parallel dipole moments of the individual layers, in the lowest energy structure of bilayer fluorographane closes the band gap and metallizes bilayer fluorographane. However, if one constructs a non-polar bilayer of fluorographane, the band gap increases to 3 eV. In this stacking type, the same terminated side of individual fluorographane layers face to each other and the net dipole moment becomes zero. Similarly, we observe that when MoS_2 is put on the hydrogenated side of fluorographane, the separation of the valence and conduction band of absorbed fluorographane increases from 2.3 eV to 3.3 eV due to the reduction of the intrinsic dipole moment of fluorographane as a result of charge transfer from fluorographane to MoS_2. This charge transfer creates a dipole moment pointing from MoS_2 to fluorographane, which is antiparallel to the intrinsic dipole moment of fluorographane. Here, we have a gap of 2.3 eV for pristine fluorographane instead of 2.6 eV because of the applied strain to the fluorographane lattice to make it commensurable with the MoS_2 lattice. Applying a 2 % strain decreases the band gap of pristine fluorographane from 2.6 eV to 2.3 eV. Depending on the local structure at the interface, the C-C bond length of bare fluorographane varies within the range of 2.49-2.60 Å.

We also investigate the effect of a perpendicular electric field on the electronic properties of the fluorographane-MoS_2 heterostructure. The concentration of charge carriers on the MoS_2 monolayer in TMDC based FETs can be tuned by an external electric field. Such electric field can be produced by a gate electrode in a real device. Figure 3 shows the *n*-type and *p*-type Schottky barrier heights at the interface of fluorographane and MoS_2 subjected to an out of plane electric field. Here, we calculate the *p*-type (*n*-type) Schottky barrier, Φ_p (Φ_n), for the MoS_2 monolayer placed on the fluorine (hydrogen) terminated side of fluorographane. As seen from Fig. 3, the application of a negative and positive electric field results in different shifts in the bands of MoS_2. For instance a negative electric field applied to the MoS_2 monolayer absorbed on the F terminated side of fluorographane makes the conduction band of fluorographane closer to the Fermi level and the valence band of MoS_2. This means that we can decrease the size of the *p*-type Schottky barrier height, and hence it is possible to attain a barrierless interface by applying a perpendicular electric field. This easy tunability of the electronic properties allows one to change the *p*-type Schottky barrier height by 1 eV. In contrast, the change in Φ_n for the MoS_2 monolayer interfaced with hydrogen terminated side of fluorographane is only 0.1 eV. As seen from Fig. 3(b), Φ_n is always negative, implying a barrierless interface. When the applied electric field switches from negative to positive, the Fermi level moves upwards within the conduction band of MoS_2, thereby increasing the carrier concentration within this band.

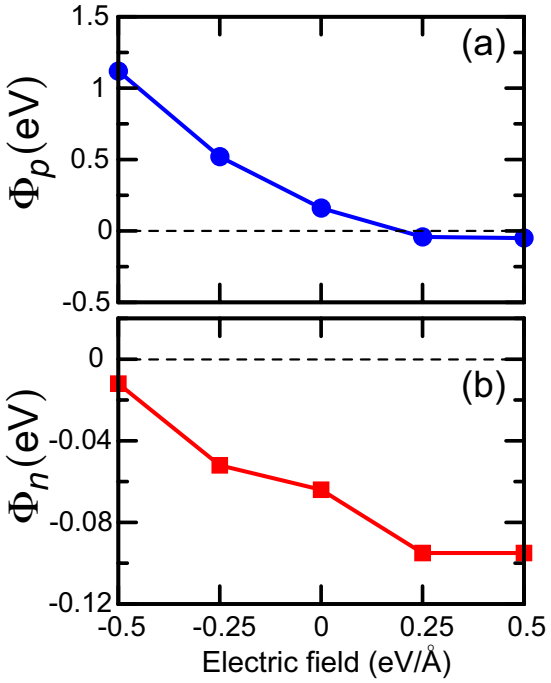

Fig. 3 The *p*- and *n*-type Schottky barriers as a function of external electric field for MoS_2 absorbed on (a) fluorine and (b) hydrogen terminated side of fluorographane, respectively. Φ_p and Φ_n denote the *p*- and *n*-type Schottky barriers, respectively.

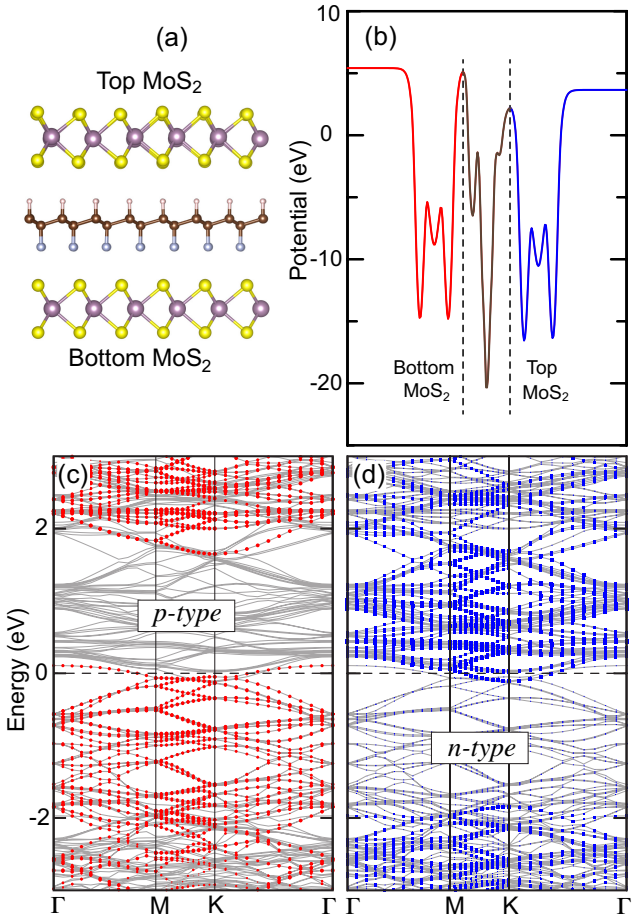

Fig. 4 (a) Optimized structure of bilayer MoS_2 separated by fluorographane. (b) Plane averaged electrostatic potential energy across the MoS_2-fluorographane-MoS_2 trilayer. Calculated band structure projected on the bottom layer in (c) and the top layer (d) MoS_2 states. Red (blue) color is used for bottom (top) MoS_2. Fermi level is at 0 eV.

5 MoS_2-Fluorographane-MoS_2 trilayer heterostructure

Finally, we investigate a bilayer of MoS_2 intercalated with a monolayer of fluorographane, see Fig. 4(a). The presence of a potential difference across the fluorographane monolayer breaks the interface symmetry and results in a *p*-type (*n*-type) doping of the bottom (top) MoS_2 monolayer. Such potential difference and the resultant dipole moment triggers a charge transfer from the bottom MoS_2 layer to the top MoS_2 layer. As a result of this charge transfer, while the conduction band of the top MoS_2 monolayer crosses the Fermi level, the valence band of the bottom MoS_2 monolayer appears at the Fermi level. Thus, to obtain such bipolar doping, we do not need to apply an external electric field. In this particular stacking, the energy gap between the valence and conduction band of fluorographane increases from 2.3 eV to 4.4 eV. We also calculate the plane-averaged electrostatic potential along the normal of the MoS_2-fluorographane-MoS_2 trilayer, see Fig. 4(b). A significant electrostatic potential difference of 1.75 eV is found between the bottom and top MoS_2 monolayers. Besides the intrinsic dipole moment of fluorographane, an additional dipole moment, pointing from the top MoS_2 monolayer to the bottom MoS_2 monolayer, is formed due to the charge transfer. This newly formed dipole moment is antiparallel to the dipole moment of fluorographane and weakens the strength of the latter. Such a device structure can be utilized to construct efficient *p*-*n* junctions, field effect transistors or logic devices that require to have both *n*-type and *p*-type materials together on the nanoscale.

In addition to the MoS_2-fluorographane-MoS_2 trilayer heterostructure as discussed above, we also study trilayers in which both MoS_2 monolayers are put either on the hydrogen or fluorine terminated side of fluorographane. These trilayer structures show similar electronic properties as their corresponding MoS_2-fluorographane bilayer heterostructures as is apparent from Fig. 2. Due to the presence of fluorographane, the bands of the individual MoS_2 layers shift with respect to each other by an amount of 0.15 eV. We demonstrate that the order of the monolayers in the stacking determines the electronic properties. Depending on the type of application, the electronic properties of TMDCs can be tuned by changing the type and sequence of individual monolayers in a stacking, which gives us ample opportunities for the design of new and efficient devices.

6 Conclusion

In summary, we investigated the electronic and structural properties of the fluorographane-MoS_2 heterostructure by means of first-principles calculations based on density functional theory. First of all, as a substrate, the fluorographane monolayer is a suitable choice for MoS_2. We found that the electronic properties of MoS_2 are determined by the type of termination of fluorographane. Contacting MoS_2 to the hydrogen (fluorine) terminated side of fluorographane results in a very strong *n*- (*p*-) type doping of MoS_2. This promising property, originating from the presence of an intrinsic dipole moment, of fluorographane allows us to control the type of doping of MoS_2. Due to the weak interaction between fluorographane and MoS_2, the resulting heterostructure is free of Fermi level pinning. The calculated *n*-type and *p*-type Schottky barrier heights are 0 and 0.16 eV, respectively. Applying an external electric field helps to diminish the *p*-type Schottky barrier height and to control the doping level of the MoS_2 monolayer. Finally, we show that the presence of fluorographane intercalated between two MoS_2 layers

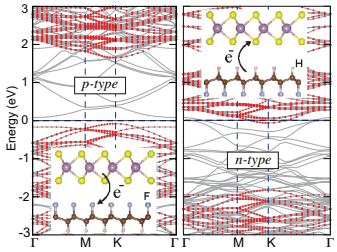

Fig. 5 TOC

initiates a charge transfer between MoS_2 layers in a MoS_2-fluorographane-MoS_2 trilayer. This charge transfer makes it possible to realize both *n*- and *p*-type doped materials together, which is a vital requirement for several device applications.

7 Acknowledgments

This work was supported by the Flemish Science Foundation (FWO-Vl) and the Methusalem foundation of the Flemish government. Computational resources were provided by TUBITAK ULAKBIM, High Performance and Grid Computing Center (TR-Grid e-Infrastructure), and HPC infrastructure of the University of Antwerp (CalcUA) a division of the Flemish Supercomputer Center (VSC), which is funded by the Hercules foundation.

References

1 J. Wilson and A. Yoffe, *Advances in Physics*, 1969, **18**, 193–335.
2 K. F. Mak, C. Lee, J. Hone, J. Shan and T. F. Heinz, *Phys. Rev. Lett.*, 2010, **105**, 136805.
3 C. Ataca, H. Şahin and S. Ciraci, *J. Phys. Chem. C*, 2012, **116**, 8983–8999.
4 Q. H. Wang, K. Kalantar-Zadeh, A. Kis, J. N. Coleman and M. S. Strano, *Nat. Nanotechnol.*, 2012, **7**, 699–712.
5 X. Song, J. Hu and H. Zeng, *J. Mater. Chem. C*, 2013, **1**, 2952–2969.
6 M. Xu, T. Liang, M. Shi and H. Chen, *Chem. Rev.*, 2013, **113**, 3766–3798.
7 X. Huang, Z. Zeng and H. Zhang, *Chem. Soc. Rev.*, 2013, **42**, 1934–1946.
8 M. Chhowalla, H. S. Shin, G. Eda, L.-J. Li, K. P. Loh and H. Zhang, *Nat. Chem.*, 2013, **5**, 263–275.
9 D. Jariwala, V. K. Sangwan, L. J. Lauhon, T. J. Marks and M. C. Hersam, *ACS Nano*, 2014, **8**, 1102–1120.
10 D. Çakır, F. M. Peeters and C. Sevik, *Applied Physics Letters*, 2014, **104**, 203110.
11 F. A. Rasmussen and K. S. Thygesen, *The Journal of Physical Chemistry C*, 2015, **119**, 13169.
12 H. Wang, H. Feng and J. Li, *Small*, 2014, n/a–n/a.
13 B. Radisavljevic, A. Radenovic, J. Brivio, V. Giacometti and A. Kis, *Nat. Nanotechnol.*, 2011, **6**, 147.
14 S. Larentis, B. Fallahazad and E. Tutuc, *Appl. Phys. Lett.*, 2012, **101**, 223104.
15 W. Liu, J. Kang, D. Sarkar, Y. Khatami, D. Jena and K. Banerjee, *Nano Lett.*, 2013, **13**, 1983–1990.
16 A. Dankert, L. Langouche, M. V. Kamalakar and S. P. Dash, *ACS Nano*, 2014, **8**, 476–482.
17 S. Das, H.-Y. Chen, A. V. Penumatcha and J. Appenzeller, *Nano Lett.*, 2013, **13**, 100–105.
18 W. Chen, E. J. G. Santos, W. Zhu, E. Kaxiras and Z. Zhang, *Nano Lett.*, 2013, **13**, 509–514.
19 W. Liu, J. Kang, D. Sarkar, Y. Khatami, D. Jena and K. Banerjee, *Nano Lett.*, 2013, **13**, 1983–1990.
20 J. Kang, W. Liu and K. Banerjee, *Appl. Phys. Lett.*, 2014, **104**, 093106.
21 I. Popov, G. Seifert and D. Tománek, *Phys. Rev. Lett.*, 2012, **108**, 156802.
22 J. Kang, D. Sarkar, W. Liu, D. Jena and K. Banerjee, *IEEE International*, 2012, 17.4.1–17.4.4.
23 J. Kang, W. Liu, D. Sarkar, D. Jena and K. Banerjee, *Phys. Rev. X*, 2014, **4**, 031005.
24 D. Çakır and F. M. Peeters, *Phys. Rev. B*, 2014, **89**, 245403.
25 C. Gong, L. Colombo, R. M. Wallace and K. Cho, *Nano Lett.*, 2014, **14**, 1714–1720.
26 J.-R. Chen, P. M. Odenthal, A. G. Swartz, G. C. Floyd, H. Wen, K. Y. Luo and R. K. Kawakami, *Nano Lett.*, 2013, **13**, 3106–3110.
27 A. Dankert, L. Langouche, M. V. Kamalakar and S. P. Dash, *ACS Nano*, 2014, **8**, 476–482.
28 D. Çakır, C. Sevik and F. M. Peeters, *J. Mater. Chem. C*, 2014, **2**, 9842–9849.
29 S. Kim, A. Konar, W.-S. Hwang, J. H. Lee, J. Lee, J. Yang, C. Jung, H. Kim, J.-B. Yoo, J.-Y. Choi, Y. W. Jin, S. Y. Lee, D. Jena, W. Choi and K. Kim, *Nat Commun*, 2012, **3**, 1011.
30 M. Farmanbar and G. Brocks, *Phys. Rev. B*, 2015, **91**, 161304.
31 C. He, W. X. Zhang, T. Li, L. Zhao and X. G. Wang, *Phys. Chem. Chem. Phys.*, 2015, –.
32 T. Musso, P. V. Kumar, A. S. Foster and J. C. Grossman, *ACS Nano*, 2014, **8**, 11432–11439.
33 K. S. Novoselov, A. K. Geim, S. V. Morozov, D. Jiang, S. C. Dubonos, I. V. Grigorieva and A. A. Firsov, *Science*, 2004, **306**, 666.
34 K. S. Novoselov and A. K. Geim, *Nat. Mater.*, 2007, **6**, 183.
35 A. H. Castro Neto, F. Guinea, N. M. R. Peres, K. S. Novoselov and A. K. Geim, *Rev. Mod. Phys.*, 2009, **81**, 109–162.
36 H. Sahin, O. Leenaerts, S. K. Singh and F. M. Peeters, *Wiley Interdisciplinary Reviews: Computational Molecular Science*, 2015, **5**, 255–272.
37 Z. Sofer, P. Simek, V. Mazanek, F. Sembera, Z. Janousek and M. Pumera, *Chem. Commun.*, 2015, **51**, 5633–5636.
38 P. V. C. Medeiros, A. J. S. Mascarenhas, F. de Brito Mota and C. M. C. de Castilho, *Nanotechnology*, 2010, **21**, 485701.
39 R. Paupitz, P. A. S. Autreto, S. B. Legoas, S. G. Srinivasan, A. C. T. van Duin and D. S. Galvo, *Nanotechnology*, 2013, **24**, 035706.
40 Z. Liu, R.-Z. Wang, L.-M. Liu, W.-M. Lau and H. Yan, *Phys. Chem. Chem. Phys.*, 2015, **17**, 11692–11699.
41 M. T. Ong, K.-A. N. Duerloo and E. J. Reed, *The Journal of Physical Chemistry C*, 2013, **117**, 3615–3620.
42 H. J. Kim, M. Noor-A-Alam, J. Y. Son and Y.-H. Shin, *Chemical Physics Letters*, 2014, **603**, 62 – 66.
43 G. Kresse and J. Furthmüller, *Phys. Rev. B*, 1996, **54**, 11169–11186.
44 G. Kresse and D. Joubert, *Phys. Rev. B*, 1999, **59**, 1758–1775.
45 G. Kresse and J. Hafner, *Phys. Rev. B*, 1993, **47**, 558–561.
46 H. J. Monkhorst and J. D. Pack, *Phys. Rev. B*, 1976, **13**, 5188–5192.
47 S. Grimme, *J. Comput. Chem.*, 2006, **27**, 1787–1799.
48 L.-F. Wang, T.-B. Ma, Y.-Z. Hu, Q. Zheng, H. Wang and J. Luo, *Nanotechnology*, 2014, **25**, 385701.
49 H. Qiu, L. Pan, Z. Yao, J. Li, Y. Shi and X. Wang, *Appl. Phys. Lett.*, 2012, **100**, 123104.
50 V. Heine, *Phys. Rev.*, 1965, **138**, A1689–A1696.
51 S. G. Louie and M. L. Cohen, *Phys. Rev. Lett.*, 1975, **35**, 866–869.
52 H. Hasegawa and T. Sawada, *Thin Solid Films*, 1983, **103**, 119 – 140.

53 H.-P. Komsa, S. Kurasch, O. Lehtinen, U. Kaiser and A. V. Krasheninnikov, *Phys. Rev. B*, 2013, **88**, 035301.
54 W. Zhou, X. Zou, S. Najmaei, Z. Liu, Y. Shi, J. Kong, J. Lou, P. M. Ajayan, B. I. Yakobson and J.-C. Idrobo, *Nano Letters*, 2013, **13**, 2615–2622.
55 S. McDonnell, R. Addou, C. Buie, R. M. Wallace and C. L. Hinkle, *ACS Nano*, 2014, **8**, 2880–2888.
56 F. Giannazzo, G. Fisichella, A. Piazza, S. Agnello and F. Roccaforte, *Phys. Rev. B*, 2015, **92**, 081307.
57 F. Li and Y. Li, *J. Mater. Chem. C*, 2015, **3**, 3416–3421.